Biol. Cybern. 90, 165–175 (2004)
DOI 10.1007/s00422-003-0456-0

Biological Cybernetics

Otolith responses to dynamical stimuli: results of a numerical investigation

R. Jaeger[1], **T. Haslwanter**[1,2]

[1] Department of Neurology, University Hospital Zürich, Frauenklinikstr. 26, 8091 Zürich, Switzerland
[2] Institut of Theoretical Physics, ETH Zürich, Frauenklinikstr. 26, 8091 Zürich, Switzerland

Received: 13 November 2002 / Accepted: 17 November 2003 / Published online: 4 March 2004

Abstract. To investigate the dynamic effects of external forces on the displacement of the otolith membrane and subsequent neuronal responses of otoliths, we performed numerical analyses of otolith membrane displacements. In these studies we included the full geometry of the human otolith maculae, including their 3D curvature. The first part focuses on mechanical aspects of the otolith membrane. While it was found that the mechanical coupling of distant parts of the otolith membrane is only weak, these simulations indicate that curvature may have considerable local effects on displacements. They further suggest that the movements of the otoconia, embedded in the interotoconial matrix, show a resonance in a range between 100 and 2000 Hz. In the second part of the article we also investigate the tonic-phasic responses in the vestibular nerve emanating from hair cells in the striola region. Small head tilts away from head upright position are used. The simulations indicate that the direction of head tilt is coded in characteristic response patterns along the striola.

1 Introduction

The task of our sensory systems looks quite simple: they have to tell us what we are doing (i.e., standing upright or lying on the ground) and what is happening around us. Studies investigating how the different sensory inputs achieve this goal have shown that sensory systems work efficiently, exploiting all information available. For example, the auditory system is optimized to the point that any "improvement" in hearing would transduce the Brownian motion of the particles in the inner ear as acoustic noise. For the visual and the auditory systems, a detailed understanding has been achieved by presenting different stimuli: by presenting light dots at different locations we can excite different retinal ganglion cells, and by playing sounds with different frequencies we can stimulate different locations on the basilar membrane. For the balance system, however, selective stimulation of the individual areas of the sensory epithelia does not occur for any kind of head movement. Since we can only move the head as a whole, transducers of rotations about certain axes (semicircular canals) or linear accelerometers (otoliths) receive information from all parts of their epithelia. Investigations have largely succeeded in describing the transduction properties of the semicircular canals where all hair cells in a crista ampullaris have similar on-directions, i.e., they are maximally excited by rotations about a certain fixed axis. Our understanding of the semicircular canals has also benefited significantly from theoretical investigations of their mechanics, which have, for example, shown that even plugged canals can exhibit significant responses to high-frequency oscillations (Damiano and Rabbitt 1996).

In contrast, any given linear translation elicits a complicated pattern of responses on the otolith epithelium as indicated by the diversity of neural responses to head tilts (Fernandez et al. 1972). Compared with the semicircular canals, the transformation of linear accelerations into neural signals also depends on the more complicated geometry and the arrangement of hair cell on-directions on the epithelium.

Here we investigate the effects of the 3D otolith geometry on the responses to time-dependent linear accelerations with a numerical model that accounts for the basic mechanical and physiological properties of the otoliths. The otoliths, utricle and saccule are located in the inner ear labyrinth (Fig. 1). Their epithelia are made up of hair cells and connective tissue that is tightly attached to the temporal bone. Superimposed on this epithelium is the otolith membrane, and the whole structure is covered by inner ear endolymph fluid. The utricle and saccule have distinctly different boundaries: while the saccule resembles an inverted L, the utricle has a more compact kidneylike shape. Contrary to long-standing assumptions, they are not planar but show substantial curvature (Curthoys et al. 1999; Takagi and Sando 1988). Otoliths are organized structurally in several layers with different

Correspondence to: R. Jaeger
(e-mail: rudi_jaeger@web.de)

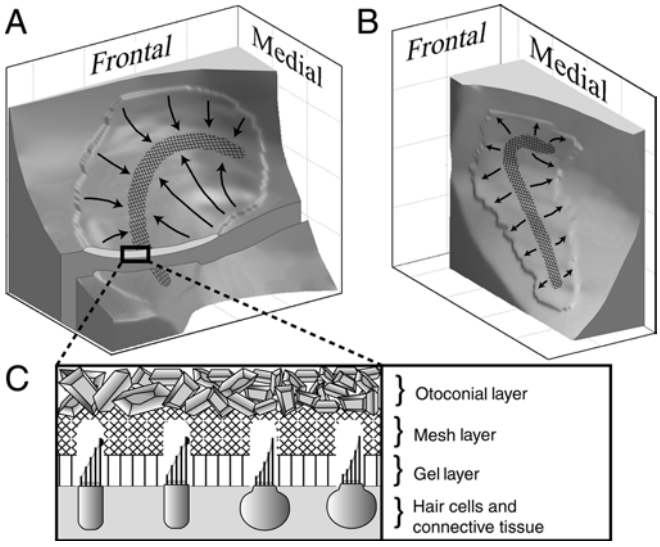

Fig. 1. View of the macular surfaces of left (**a**) utricle and (**b**) saccule. *Shaded regions* show the location of the striola, and *arrows* indicate the direction of the hair cell polarization. **(c)** Internal structure of the otoliths

mechanical properties. One of their most remarkable features (indicated in the word ''oto-lith'', or ''ear-stone'') are the otoconia crystals embedded in the topmost layer. The density of these crystals is higher than that of the surrounding materials, and linear accelerations of the head therefore result in forces leading to their displacement. The movement of the otoconia affects the otolith membrane, which is mechanically coupled to them. Shearing displacements of the membrane with respect to the underlying epithelium are sensed by hair cells located in the epithelium and subsequently signaled to the brain via the vestibular nerve.

Single otolith afferent nerve fibers exhibit responses that can be either ''tonic'' or ''tonic-phasic'' (Goldberg et al. 1990a). Due to their response properties, tonic units are believed to respond proportionally to membrane displacements (Grant et al. 1994) and dominate in the lateral parts of the otoliths (Goldberg et al. 1990b). Tonic-phasic units are found predominantly along a bandlike region in the central part of the otoliths, the ''striola'' (Fig. 1). They are especially interesting for information processing since they provide dynamic information about movements. Since little quantitative information is available about regional variations of the physiological and transduction properties of otolith hair cells, as well as of interconnections further downstream, we approximate the neural responses of such cells by using their known mean-response curves in the frequency domain (Goldberg et al. 1990a).

2 Methods

2.1 Physiology

2.1.1 Otolith structure. Though it has been known for a long time that otoliths sense linear accelerations of the head, a detailed view of the mechanical properties has been hampered by the difficulty of fixating otolith tissue (Lindeman 1969; Lins et al. 2000). We based our model on the finding that three morphologically different sublayers can be found in the otolith membrane (Kachar et al. 1990; Ross et al. 1987) (Fig. 1): First the gel layer, which is closest to the apical surface of the hair cells, then the mesh layer, and on top the otoconial layer. Note that different terminologies are used for the individual layers.

The gel layer has viscoelastic properties and is commonly treated as a Kelvin-Voight fluid (Grant et al. 1990). Since the mechanical sensors of the hair cells, i.e., the hair bundles, are embedded in the gel layer, the elasticity and viscosity of this layer have a large effect on the neural otolith response. The elasticity of the gel layer has been attributed to a columnar filament structure and to the hair bundles (Benser et al. 1993). We assumed a constant height of 10 μm for this layer. The second layer, which we call the ''mesh layer'', is much stiffer than the gel layer. It is made up of a densely connected isotropic filament mesh and also has a height of about 10 μm. Mechanically, this layer probably acts to disperse high local otoconial forces over a wider area. The otoconia are embedded in the uppermost part of the otolith membrane, labeled ''otoconial layer'' in Fig. 1. They are connected to each other and the underlying mesh layer through an interotoconial filament matrix (Kachar et al. 1990). We assumed a height of 15 μm for this layer.

The calculations presented here include the geometry of human macular surfaces, which were obtained from reconstructed slices of the inner ear (Sato et al. 1992; Takagi and Sando 1988). They are shown in Fig. 1, with the data presented in a head-fixed coordinate system corresponding to the head upright position. Since the reconstructed slices also included the semicircular canals, we were able to ensure the proper orientation of the otoliths by calculating the unit vectors perpendicular to the planes of the semicircular canals and comparing them with published data (Blanks et al. 1975). In addition, the part of the data set that characterizes the planes of the maculae was smoothed. A detailed description of the smoothing procedure has been given in Jaeger et al. (2002).

2.1.2 Hair cells and transformation properties. Direction and magnitude of otolith membrane deflections are detected by the hair cells (Fernandez and Goldberg 1976; Shotwell et al. 1981). Short hair bundles, called ''stereocilia'', are embedded in the gel layer (Fig. 1c). They are interconnected via tip links (Hackney and Furness 1995; Howard and Hudspeth 1987) and linked to a single long hair, the ''kinocilium''. Bending of the hair bundle due to a deformation of the gel layer leads to direction-specific hyperpolarization or depolarization of the hair cell. The ''polarization vector'' indicates the direction leading to maximum depolarization. The polarization vectors of different hair cells are not randomly distributed over the epithelium but show a distinct pattern (Lindeman 1969), indicated by the

arrows in Fig. 1. Due to the curvature of the epithelium, the vectors have x, y, and z components. To obtain the 3D components of the polarization vectors, we manually created a 2D vector field according to the observations by Lindeman. This field was then projected onto the curved macula. The intracellular hair cell potential depends on the cosine of the angle between the local polarization vector and the hair cell deflection (Shotwell et al. 1981). We assumed that the hair cell potential is linearly related to the magnitude of deflection, which is justified as long as the external acceleration is smaller than about 3 g (Fernandez and Goldberg 1976).

Two types of hair cells can be distinguished morphologically – spherical type I cells and flasklike type II cells (Goldberg et al. 1990b). Hair cells are innervated by vestibular neurons situated in Scarpa's ganglion. They exhibit a resting discharge frequency of 80–100 Hz. Afferent fibers generally innervate more than one hair cell. Depending on the type of hair cells innervated, afferent fibers are termed calyx, bouton, and dimorphic units. Calyx units form connections with one or more type I hair cells and are found in the striola. Bouton units exclusively innervate type II cells and are found in the extrastriola region. Dimorphic units form connections with both types of hair cells and are found all over the epithelium.

Sinusoidal accelerations with different frequencies are usually employed to measure the responses in terms of changes of the discharge frequency. These changes are usually scaled by the amplitude of the acceleration present for a specific stimulus frequency. The resulting gain and phase values characterize the vestibular response to time-dependent acceleration stimuli.

In this paradigm, units exhibit different responses depending on their location on the epithelium (Goldberg et al. 1990b). Striolar units show transient, tonic-phasic responses and large gain increases as the frequency of the stimulus is increased. In contrast, units in the extrastriola region typically exhibit tonic responses with only small gain enhancements (Goldberg et al. 1990a). It is thought that tonic responses are proportional to the amount of kinocilium deflections, while tonic-phasic units are also sensitive to the time rate of the deflection (Hess 1992). Responses of both types of units vary around a mean response, with larger variations for tonic-phasic units. To our knowledge these variations are not systematically associated with specific regions on the epithelium. Consequently, previous descriptions of the frequency dependence of gain and phase in the form of transfer functions were related to the mean responses (Goldberg et al. 1990a; Grant et al. 1994). Goldberg et al. introduced a transfer function H(s) that was formed by multiplying the three parts $H_M(s)$, $H_V(s)$, and $H_A(S)$ (Goldberg et al. 1990a). $H_M(s)$ reflects the mechanics of the otolith membrane, $H_V(s)$ incorporates the transformations of the response by the hair cells and their afferent connections, and $H_A(s)$ describes adaptive components. Only $H_A(s)$ has been measured directly. Goldberg et al. found the other functions and their respective parameters by fitting them to measured data. When we compared the transfer functions predicted by our simulations with the mechanical transfer functions $H_M(s)$ from Goldberg et al., we found that the two were similar in the range between 0.1 and 10 Hz. Since the results regarding hair cell dynamics are qualitative, no attempts were made to readjust the parameters of $H_V(s)$, and we employed the same functions $H_V(s)$, $H_A(s)$ and their respective parameters as Goldberg et al. in this investigation.

Since the response depends on the direction of the stereocilia displacement as well as its magnitude, we calculated an "effective displacement" (ED) by

$$ED \propto \boldsymbol{p} \cdot \boldsymbol{u} = |\boldsymbol{u}| \cos(\boldsymbol{p}, \boldsymbol{u}) \qquad \text{with} \quad |\boldsymbol{p}| = 1$$

for every location on the striola and point in time. Here $\boldsymbol{p}$ is the normalized polarization vector, $\boldsymbol{u}$ the displacement of the otolith membrane at the border between gel and mesh layer, and "$\cdot$" the scalar product. Following Grant et al. (1994) we assumed that the hair cells sensed the direction and magnitude of the displacement at the gel/mesh layer boundary. The manual adjustment of the directions of the polarization vectors induced small discontinuities in the ED. To reduce this local effect as well as numerical inaccuracies, we applied a moving average filter on neighboring striola points to smooth the ED. The resulting time series were transformed into the frequency domain and multiplied by $H_V(s)$ and $H_A(s)$, as found by Goldberg et al. for tonic-phasic units. The inverse transformation yielded the responses in the time domain. As the original derivation of H(s) used a DC gain that was scaled to unit magnitude, responses are proportional to mean vestibular firing rates.

Since the present study was interested primarily in the dynamic response patterns of striola units based on the 3D geometry of the epithelium, we did not include details of the micromechanics of vestibular hair cells. Similarly, empirical models of otolith membrane mechanics can lead to a better approximation of experimental data than the approach in this investigation (Goldberg et al. 1990a; Grant et al. 1994). Since the additional gain changes vary smoothly and by $\leq 20\%$, they would not lead to qualitative changes of the predicted response patterns.

2.2 Theory

2.2.1 Continuum mechanics. We modeled the mechanical properties of the otolith membrane as a linearly elastic, isotropic material. Though it is known that the gel layer is anisotropic, we believe that this is a valid approach. Based on morphological investigations (Kachar et al. 1990), we assume that the main anisotropy arises from a higher stiffness of the columnar filament in the direction perpendicular to the epithelium, compared to a lower stiffness in directions parallel to the epithelium. Since the displacement of the gel layer is largely due to shear forces parallel to the epithelium, the increased stiffness in the perpendicular direction probably has only a small effect. Based on the linear relationship between acceleration and neural responses for accelerations smaller than 2–3 g in tonic units (Fernandez and Goldberg 1976;

Fernandez et al. 1972), we further assumed that nonlinear effects in the viscoelastic properties of the materials could be ignored. Simulations by other groups that also used these assumptions have demonstrated that this leads to results that are in close correspondence with experimental findings (Grant and Cotton 1990; Kondrachuk 2000). In this case, the equation governing the displacement of a small part of the membrane is

$$\rho \frac{\partial^2 \boldsymbol{u}}{\partial t^2} = \rho_{\text{eff}} \overrightarrow{\text{Acc}} + (\mu_{\text{el}} + \lambda_{\text{el}}) \nabla e + \mu_{\text{el}} \Delta \boldsymbol{u} + (\mu_{\text{visc}} + \lambda_{\text{visc}}) \nabla \frac{\partial e}{\partial t} + \mu_{\text{visc}} \Delta \frac{\partial \boldsymbol{u}}{\partial t} \quad . \tag{1}$$

The variables "$\boldsymbol{u}$" and "t" denote spatial displacement and time, respectively, and $e = div\ \boldsymbol{u}$. ρ indicates the density of the material and ρ_{eff} its effective density (i.e., the difference between ρ and the density of the endolymph fluid). If ρ_{eff} is different from zero, as in the case of the otoconial layer, accelerations $\overrightarrow{\text{Acc}}$ produce forces within the otolith membrane. The elastic properties of an isotropic, linear material can be described using the two "Lamé parameters", λ and μ. λ_{el} and μ_{el} are the Lamé constants that characterize the elastic properties of the material, and λ_{visc} and μ_{visc} describe the damping aspects of the continuum. They are associated with terms that include the time derivative of $\boldsymbol{u}$ (i.e., the velocity of displacements). Equation (1) can be used to model all layers of the otolith membrane by choosing appropriate material parameters.

We used standard finite element techniques (Rao 1982) to solve (1). The volume of the otolith membrane was broken down into about 1000 small hexahedrons that were placed in such a way as to ensure that they belonged to only one type of material. With finite element analysis, (1) is transformed into

$$[A] \frac{\partial^2 \boldsymbol{U}}{\partial t^2} + [B] \frac{\partial \boldsymbol{U}}{\partial t} + [C] \boldsymbol{U} = \boldsymbol{F}(t) \quad . \tag{2}$$

This is a matrix equation for all nodal degrees of freedom $\boldsymbol{U}$. For 3D displacements, the size of $\boldsymbol{U}$ is given by 3×N: "3" for the three dimensions and "N" for the number of nodes. The vector $\boldsymbol{U}$ incorporates the 3D displacements at all nodes. [A] is called the "mass matrix" since it is associated with the nodal accelerations, [B] the "damping matrix", and [C] the "stiffness matrix". The time-dependent function $\boldsymbol{F}(t)$ characterizes the external force on the system. To determine the system completely, boundary conditions need to be specified. In our model, the nodes at the gel/epithelium border were not allowed to move (i.e., those points were fixed), and no interaction was assumed at the boundary between endolymph fluid and the otolith membrane.

Commonly, the damping matrix [B] is constructed as a linear superposition of the mass and the stiffness matrix (Rayleigh damping):

$$[B] \ = \ \alpha[A] + \beta[C] \quad . \tag{3}$$

The parameters α and β determine to which degree [A] and [C] participate in the damping matrix. We used stiffness proportional damping only (i.e., $\alpha = 0$).

Equation (2) is a differential equation in time. We used two methods to integrate the equation. For the tilt experiments, we employed a direct integration scheme. Starting from a nondeformed and nonmoving initial configuration, displacements, velocities, and accelerations at subsequent time steps were calculated. By taking the configuration of the previous step as the initial condition, the dynamic state of the system at the next time step was calculated. Equation (2) can also be solved with the "mode superposition" method, where the free-vibration mode shapes of the finite element structure are used to calculate its mechanical response. The response is then described as a superposition of these mode shapes. We used mode superposition to find the transfer functions of the otolith membrane. The calculations were performed with "Abaqus", a commercial finite-element software package (Hibbitt, Karlsson & Sorensen, Inc., Rhode Island, USA).

2.2.2 Mechanical transfer function. For an externally applied sinusoidal acceleration, the otolith system reacts with a sinusoidal movement. The frequency-dependent displacement amplitudes and phase shifts relative to the acceleration characterize the system. For an infinitely extended planar otolith, Grant et al. (1994) derived an analytical solution. They assumed a two-layered membrane: an otoconial and a gel layer, covered by endolymph fluid. We extended this approach to a three-layer system by including an intermediate mesh layer (Fig. 1). The transfer function is

$$\frac{\delta}{\text{Acc}} = \frac{l_{\text{oto}} \rho_{\text{oto}}^{\text{eff}}}{(\rho_{\text{oto}} bs + \mu_{\text{visc}}^{\text{fluid}} c) s\sigma + (\mu_{\text{el}}^{\text{mesh}} + \mu_{\text{visc}}^{\text{mesh}} s)\gamma} \tag{4}$$

with

$$\gamma = -\frac{a}{\sinh(a l_{\text{mesh}})} + \sigma a \coth(a l_{\text{mesh}}) \quad ,$$

$$\sigma = \frac{a}{b} \coth(b l_{\text{gel}}) \sinh(a l_{\text{mesh}}) + \cosh(a l_{\text{mesh}}) \quad ,$$

and

$$a = \sqrt{\frac{\rho s^2}{\mu_{\text{el}}^{\text{mesh}} + \mu_{\text{visc}}^{\text{mesh}} s}} \ ;$$

$$b = \sqrt{\frac{\rho s^2}{\mu_{\text{el}}^{\text{gel}} + \mu_{\text{visc}}^{\text{gel}} s}} \ ;$$

$$c = \sqrt{\frac{\rho s}{\mu_{\text{visc}}^{\text{fluid}}}} \quad ,$$

where δ indicates the displacement at the gel/mesh layer boundary, Acc, ρ_{oto}, and $\rho_{\text{oto}}^{\text{eff}}$ are external acceleration, otoconia density, and effective density of the otoconial layer, respectively. The heights of the three layers are characterized by l_{oto} for the otoconial layer, l_{mesh} for the mesh layer, and l_{gel} for the gel layer. Elastic properties of the system are indicated by $\mu_{\text{el}}^{\text{mesh}}$ and $\mu_{\text{el}}^{\text{gel}}$, which are the shear moduli of the mesh and gel layers, respectively. $\mu_{\text{visc}}^{\text{fluid}}$, $\mu_{\text{visc}}^{\text{mesh}}$, and $\mu_{\text{visc}}^{\text{gel}}$ are the viscosity of the endolymph

fluid, the mesh layer, and the gel layer, respectively. The density of the endolymph fluid is characterized by ρ. We assumed that all parts of the system except the otoconial layer have this density. Equation (4) depends on the Laplace transform variable s. By multiplying this equation by Acc we obtain the frequency-dependent magnitude of displacement at the gel/mesh layer boundary, as well as the corresponding phase shift.

2.3 Mechanical parameters

The analysis of mechanical properties of the otolith membrane requires the specification of appropriate mechanical parameters for the different layers. For the density of the gel and mesh layers we took 1.0 g/cm^3, which is close to the density of the endolymph fluid. Therefore, these layers are not subject to external accelerations (1). Otoconia crystals have a density of 2.7 g/cm^3 (Money et al. 1971). They are embedded in the interotoconial matrix, which has a lower density and leads to a density of about 2.0 g/cm^3 for the otoconial layer (Trincker 1962).

The properties of elastic materials are often given in terms of "Young's modulus" E and "Poisson ratio" v, instead of the Lamé parameters. They are related to each other by

$$E = \frac{\mu(3\lambda + 2\mu)}{\lambda + \mu} \quad \text{and} \quad v = \frac{\lambda}{2(\lambda + \mu)} \ . \tag{5}$$

We assumed that all parts of the otolith membrane are virtually incompressible and used a Poisson ratio of 0.49. (Completely incompressible materials have a Poisson ratio of 0.5.)

Due to the small size of the otoliths and preparation problems, Young's modulus for the gel, mesh, and otoconial layers are hard to measure. Calculations point to a value of about 10 Pa for the gel layer of mammals (Kondrachuk 2001a). The elasticity of the mesh layer is not available for mammals. For the bullfrog, Kondrachuk (2000), based on experimental data from Benser et al. (1993), found an elasticity ratio ($E_{\text{Mesh}}/E_{\text{Gel}}$) of about 20. Using this ratio, we obtained a Young modulus of 200 Pa for the mesh layer. Less is known about the elasticity of the otoconial layer. It is unclear how the elasticity is affected by the distribution of the otoconia. It is generally believed that otoconia crystals are distributed randomly within the layer, although Lindeman (1969) found that they are organized in layers. Lindeman also pointed out that crystals in the extrastriola region are larger than in the striola. While the crystals consist of hard materials and may be treated as rigid bodies in this investigation, observations suggest that the elasticity of the interotoconial matrix is considerably lower than the corresponding parameter of the mesh layer (Lins et al. 2000). The mechanical properties of the otoconial layer are thus determined by the properties of the otoconia, their distribution within the layer, and the interotoconial matrix. Since the interotoconial matrix is a rather weak structure, its purpose may be to keep the otoconia in place while allowing substantial flexibility of the layer. To reflect this property in the simulation, we chose a rather small Young modulus of 10 Pa for this layer, which is identical to the elasticity of the gel layer.

The effects of damping are measured by the viscosity parameter. Gels in general show a frequency dependence of the viscosity. We did not include such a relation in our model because results of other studies have indicated that the viscous properties of the gel layer can be modeled reasonably by a proportional model (Goldberg et al. 1990a; Grant et al. 1994). Estimates of the shear viscosity of the gel layer that were based on electrophysiological studies (Goldberg et al. 1990a) range between 0.1 Poise (Grant et al. 1994) and 1.0 Poise (Kondrachuk 2000). We used an intermedial gel layer viscosity of 0.3 Poise. As mentioned above, stiffness-proportional Rayleigh damping was employed. From (3) and a viscosity of 0.3 Poise, we obtained for β a value of 0.01 s. We used the same value to model the mesh layer since this value has not been measured and the effects of damping should be small in this layer. Apart from the investigation into the resonance properties of the otoconial layer, we did not include damping in this layer because its structure differs from that of the other two layers.

3 Results

3.1 Mechanical results

3.1.1 Curvature effects on otolith dynamics. We previously found that distant parts of the otolith structure interact only weakly during static displacements (Jaeger et al. 2002). We therefore studied the dynamic effects of otolith curvature by investigating a comparatively small, quadratic section of the otoliths (300 μm × 300 μm). The planar otolith section was deformed in such a way that the curved otolith region represented a section of a sphere with radius R (Fig. 2). This deformed structure was then oscillated sinusoidally, parallel to the tangent of the layers in the central region of the section, with a maximum acceleration of 1 g and a frequency between 0.1 and 10 Hz. This frequency range covers all typical head movements (Viirre and Demer 1997). Due to the assumed incompressibility of the otolith membrane, accelerations perpendicular to the layers produce virtually no effect.

Figure 2 shows the transfer functions of the analytical solution (4) and the numerical results for the planar and deformed otolith sections. It depicts the magnitude and phase of the displacements at the gel/mesh layer boundary in the central region of the section. In all cases the phase shift is almost identical. The uppermost trace represents the amplitude of the planar sample, which coincides almost perfectly with the analytical solution. The lower traces indicate that for decreasing curvature radii the displacement amplitude is progressively reduced. Figure 3a shows the relation between displacement amplitude and curvature radius. While for a radius above 1000 μm the amplitude reduction is $< 10\%$

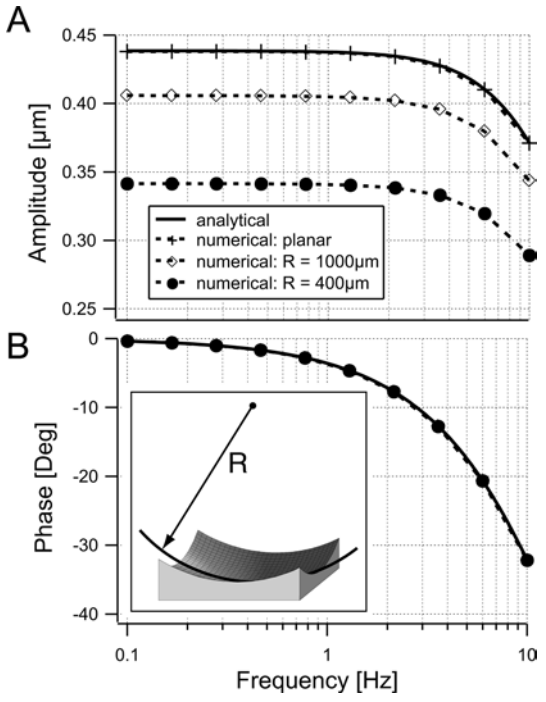

Fig. 2. Transfer function of a quadratic otolith section at the gel/mesh layer boundary. **a** While the displacements are identical for the planar section and the analytical case (*solid line*), finite curvature of the section leads to a reduction of the displacement. **b** The phase shifts are unaltered by the magnitude of the curvature radius R. The inset illustrates the definition of this parameter

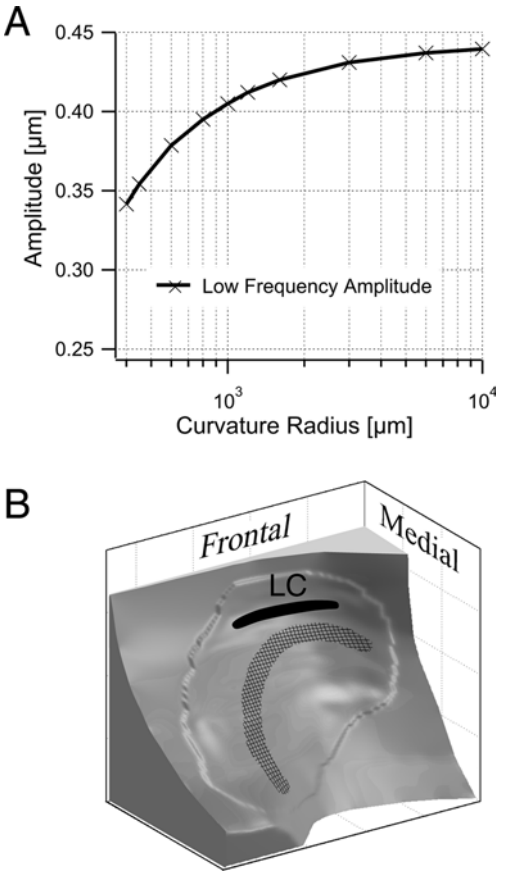

Fig. 3. **a** Dependence of the displacement amplitude at low frequencies on the curvature radius. **b** Region on the utricle where large curvature (LC) can be found. LC corresponds to a small curvature radius

compared to the planar sample, it is more pronounced for smaller radii. Based on the data set used in this investigation, we found that the radius of curvature in most areas is larger than 1000 μm. However, a small region on the utricle, marked in Fig. 3b as "large curvature area" (LC), shows a local curvature radius of about only 400 μm. Note that curvature is defined by $1/R$, where R is the curvature radius. Curvature radii in the saccule were generally above 1000 μm.

3.1.2 Effects at higher stimulation frequencies. Recent experimental findings suggest that noise and mechanical vibrations impair otoliths (Perez et al. 2002; Otsuka et al. 2003). To study the effects of higher vibration frequencies on the otolith membrane, we abandoned the simplifying assumption of isotropy in the otoconial layer (Fig. 1). If there are deformations of the otolith structure, they should be found in the vicinity of the otoconia since the gel layer is strongly damped. We constructed a simple model that included otoconia separated by an isotropic interotoconial filament matrix. For this matrix we took a density of 1.0 g/cm^3 and for the otoconia crystals a density of 2.7 g/cm^3 (Carlström et al. 1953). Since measurements of the density of the otoconial layer, i.e., otoconia plus interconnecting matrix, have shown that the combined density is about 2.0 g/cm^3 (Trincker 1962), we chose the distance between the otoconia such that it accounted for the lower density of the compounded structure. The otoconia were approximated by bricks with a basis length of 4×4 μm and a height of 6.5 μm, which were oriented in the way indicated in Fig. 4a. The height of most otoconia falls into the range of 3 to 7 μm (Lindeman 1969). To obtain the desired overall density of 2 g/cm^3, a uniform spacing of 1 μm (in all dimensions) between the otoconia (Fig. 4a) was necessary.

These are substantial simplifications with respect to the situation found in the otolith membrane. Otoconia are believed to be randomly distributed and are expected to touch each other, which would largely restrict the movement of single otoconia embedded in the structure. Nevertheless, otoconial layers with randomly or regularly distributed otoconia, as used in this investigation, share important mechanical properties. In both cases the number of otoconia found in a large volume of the layer and the space available for the elastic element (the interotoconial matrix) are similar. More accurate biomechanical models would require more quantitative information about the distribution and the mechanics of the otoconial layer.

The elastic properties of the interotoconial matrix directly influenced the results of our simulations. Lins et al. observed that the interotoconial matrix provides weak links between individual otoconia when compared with the rigidity of the supporting mesh layer (Lins et al. 2000). By assuming that the gel layer represents a typical

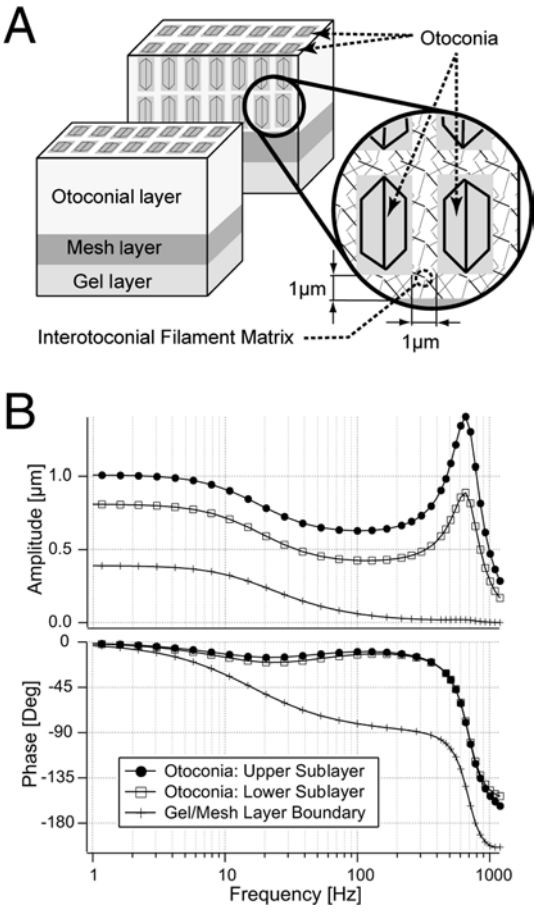

Fig. 4. Effects at higher stimulation frequencies. **a** Structure of the otolith membrane. The otoconia are separated, and the "interotoconial matrix" fills the space between them. **b** Transfer functions for the gel/mesh layer boundary (*cross*) and otoconia of the upper (*filled dots*) and lower otoconial sublayer (*open rectangles*). The otoconia show a resonance at about 650 Hz

"weak" material of the inner ear, we used elasticity constants identical to that of this layer (i.e., Young's modulus 10 Pa, and Poisson ratio 0.49) to model the interotoconial matrix. It may further be assumed that, besides the interotoconial matrix, the interotoconial space is filled with fluid, i.e., a two-phase system fills this space. Since there is no clearly defined border between the interotoconial filament and the endolymph, the endolymph fluid probably fills the interotoconial space. We chose for the viscosity of the interotoconial material a value similar to that of the endolymph fluid, 0.01 Poise, i.e., we assumed that the elasiticity of this material is provided by the filament matrix and the viscosity by the fluid. As a result, this material provided little damping. Young's modulus of the otoconia crystals was taken to be 10^{11} Pa and their Poisson ratio 0.3.

The resulting transfer functions, shown in Fig. 4b, were obtained numerically for mechanical vibrations with a maximum acceleration of 1 g. Crosses indicate the amplitude and phase at the gel/mesh layer boundary in the central region of the structure, depicted in Fig. 4a. The transfer function in this zone is very similar to the corresponding result without separated otoconia (Fig. 2): frequency independence below 5 Hz and a reduction of the amplitude around 10 Hz, accompanied by an increasing phase lag. The amplitude approaches zero at about 100 Hz and shows only minor deviations from this value at higher frequencies.

The results were different for the otoconia. The filled dots and open rectangles in Fig. 4b indicate the transfer function of single otoconia from the central region of the upper and lower sublayers, respectively (Fig. 4a). The amplitude at lower frequencies is considerably larger than at the gel/mesh layer boundary. At around 10 Hz the displacement amplitude decreases, which can be attributed to the reduced displacements of the underlying gel layer as otoconial and gel layer move together. For frequencies around 650 Hz the otoconia resonate. The movement of the otoconial sublayers with respect to the mesh layer characterizes this resonance mode. Amplitudes are larger for the upper sublayer since upper and lower sublayers move in phase and an additional elastic element is present between the sublayers. Depending on the magnitude of the acceleration, such a resonance could lead to considerable stress within the interotoconial matrix.

3.2 Vestibular responses

Based on the displacements at the gel/mesh layer boundary, the distribution of hair cell polarization vectors, and the transfer functions $H_V(s)$ and $H_A(s)$ (Goldberg et al. 1990a), we calculated the time-dependent vestibular responses at different locations along the striola. To investigate neural responses to natural stimuli, we simulated small head tilts. Starting from an upright position, the head rotated 10° smoothly in 0.4 s to a tilted position.

Figure 5 shows the model responses for the utricle. At the beginning the head is in an upright position. At 0.2 s the head tilt starts, and at 0.6 s it finishes. Figures 5a and b present the effective displacements and neuronal responses at three locations along the striola for a tilt left ear down. The resulting response traces correspond to three sections through the surface in Fig. 5d. For all three traces, maximum responses occur simultaneously before the end of the head movement, and the decay to the tonic state is similar. Figure 5a also shows the time course of gravitational acceleration along the interaural axis (thick, solid line).

By calculating the effective displacements and corresponding neural responses for many locations along the striola, we obtained patterns of these two variables, which uniquely represent the direction of head tilts. Utricular patterns of effective displacements and neural response are shown in Figs. 5c and d for left ear down tilts. Figures 5e and f present results for nose down tilts of the same magnitude and time course. Zero on the "Position" axis corresponds to the lateral end of the left utricle, and positive values indicate the location along the bent striola. As in Fig. 5b, neural responses reach their maximum values before the end of the head movement and then approach the steady state value

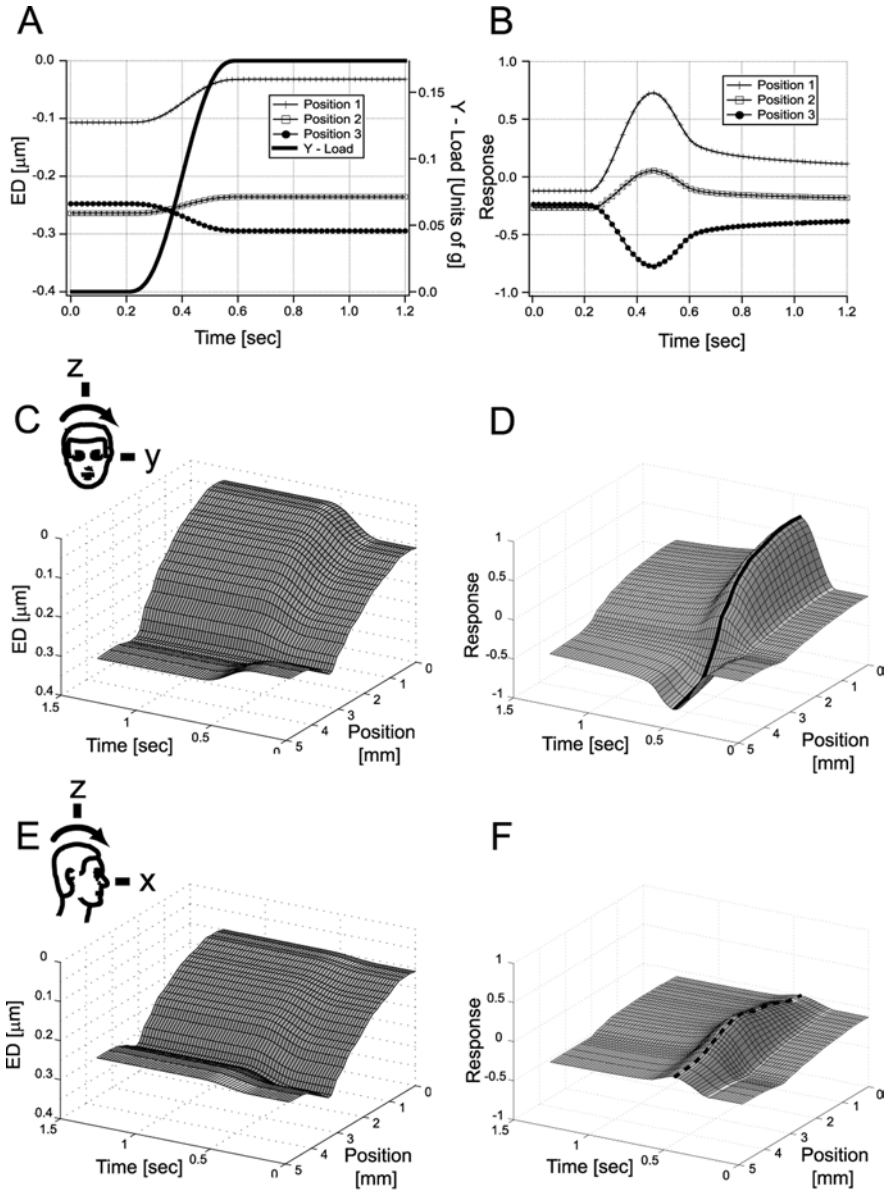

Fig. 5. Time course of mechanical and neural responses along the utricular striola during a 10° head tilt. The *left column* shows effective displacements and the *right column* neural responses along the striola. *Top row*: **a, b** Time course of effective displacements and neural responses at various position values in **c** and **d** (1, 3, and 5 mm). The *solid line* in **a** also includes the acceleration along the interaural direction (*right vertical axis*). *Middle row*: **c, d** Effective displacement (**c**) and neural response (**d**) for tilt left ear down. ''Position'' indicates the parameterized location on the striola. In the *bottom row* (**e, f**), effective displacement and neural responses are depicted for a 10° pitch tilt. The units of response magnitude are arbitrary

corresponding to the tilted head orientation. Figures 5d and f show that different tilt directions lead to clearly distinct dynamic response patterns. For a given tilt direction, however, the time courses at different striola positions are quite similar. The maximum responses, indicated in Figs. 5d and f by the thick dashed and solid line, respectively, are shown again in Fig. 6a.

Figure 6 summarizes the patterns of maximum neural response to tilts in various directions for both otoliths. For the saccule zero on the ''Position'' axis corresponds to the ventral (lower) end of the saccular striola. The thick dashed and solid lines in Fig. 6a correspond to the maximum response shown in Figs. 5d and f. The direction of 10° head tilts from upright position is characterized by an angle: 0° corresponds to forward tilt, 90° to left ear down tilt, 180° to backward tilt, and 270° to right ear down tilt.

Different tilt directions elicited different response patterns along the striolas. For example, while the lateral part of the utricle (0–1 mm) has similar response levels for tilts backward (180°) and diagonally forward (300°), the levels at the medial utricular striola are quite different. Responses varied smoothly with the tilt angle.

Though it might be expected that this kind of acceleration stimulus leads predominantly to utricular responses, we also found substantial responses for the saccule. This can be seen from Figs. 6c and d for utricle and saccule, respectively. Here the total change in response to head tilts is depicted by the integral between the initial and the maximum response along the striola. The difference between these two responses was always taken to be positive, i.e., the integration ran over the absolute value of the difference. In Figs. 6c and d, the magnitude of the total response change is plotted along the radius coordinate for every tilt direction. Large values indicate a large total response change. While total saccular responses (Fig. 6d) are generally smaller than total responses of the utricle, saccular responses still

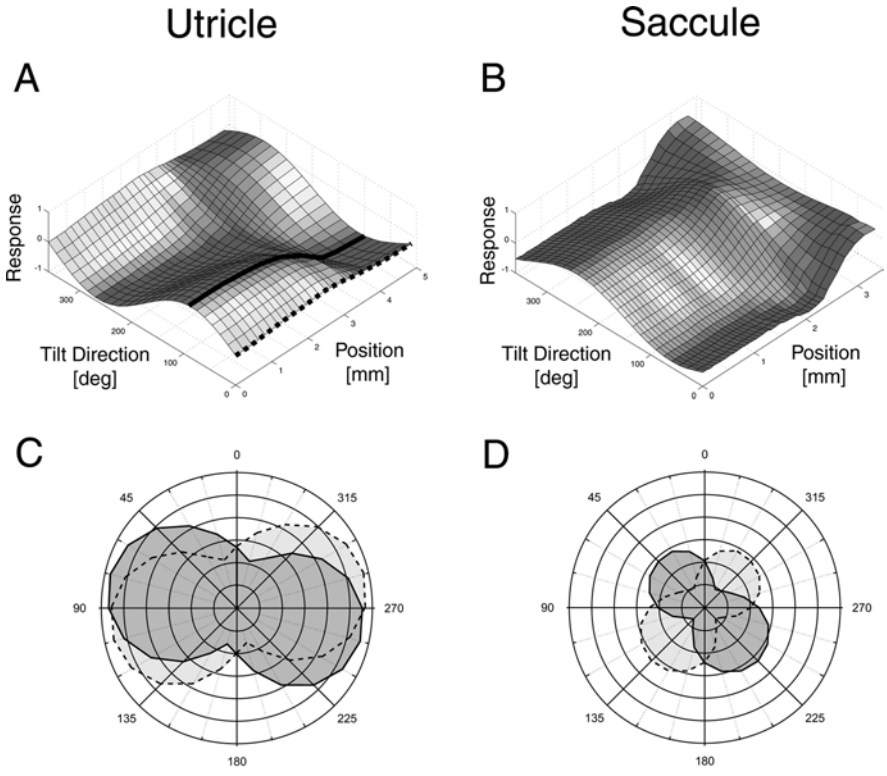

Fig. 6. Maximum responses for tilts into different directions, for utricle (*left column*, **a**) and saccule (*right column*, **b**). "Tilt Direction" 0° corresponds to nose down, 90° to left ear down tilt, etc. The *dashed* and *solid lines* in **a** correspond to the respective lines in Fig. 5d and f. "Position" is the parametric location along the striola. The *bottom row* (**c, d**) shows the absolute value of the area between the initial and the maximum response for the different tilt angles. *Dark shaded regions* correspond to the left and *light shaded regions* to the right otoliths

represent a substantial fraction of the utricular responses. For certain tilt angles (10°) total responses from the saccule and the utricle are even of similar magnitude.

4 Discussion

4.1 Mechanical results

4.1.1 Curvature effects on otolith dynamics. Few studies have investigated the dynamic behavior of the otolith membrane (Grant and Best 1987; Grant and Cotton 1990; Grant et al. 1994; Kondrachuk 2001b). These studies were based on a number of simplifying assumptions: they assumed that the otolith membrane consists of only two individual sublayers with different mechanical properties and is planar. The present study eliminates these assumptions.

In accordance with experimental findings (Kachar et al. 1990), we subdivided the otolith membrane into three different layers, i.e., we added a stiff intermediate mesh layer to the otolith structure. Both the finite-element response and the analytical transfer function that we derived showed that for flat parts of the otoliths the mesh layer does not change the movement characteristics of the gel layer compared to the model described by Grant et al. (1994). The displacement amplitude remains constant for frequencies up to 1 Hz and decreases to zero for higher frequencies, while the phase shift gradually increases. Numerical and analytically derived transfer functions differ with respect to the treatment of the endolymph fluid. While the analytical solution incorporates velocity-dependent forces of the endolymph on the otolith membrane, the finite-element approach does not. The similarity in the predicted responses suggests that viscous forces from the endolymph have only minor effects on otolith displacements in the frequency range of typical head movements.

For the three-dimensional shape of the otoliths, we used experimentally measured data from human otoliths (Sato et al. 1992; Takagi and Sando 1988). Static investigations of otolith membrane displacements that were based on these data sets indicated that the local displacements are largely determined by the local orientation of the membrane (Jaeger et al. 2002). This allowed us to study the effects of curvature on otolith displacements on small, quadratic slices. Our results indicate that curvature changes the response properties. While the phase shift remains identical to the planar case, the amplitude is reduced over the whole frequency range. This can be explained by the fact that elements outside the central region of the quadratic slice are not subject to the optimal, parallel acceleration. Instead, their displacement depends on the local orientation. Since the deflections in the neighboring parts are smaller, the displacement in the central region is reduced, too. This reduction increases as the radius of curvature becomes smaller. For most areas of the human otoliths, the curvature radius is $> 1000\mu m$, and the amplitude reduction is less than 10%. However, on the utricle we also found a region where the radius is substantially smaller (Fig. 3b). Interestingly, this region of large curvature is close to the striola and shows a similar orientation. Since other researchers have put the striola more frontally and laterally than Lindeman did (Flock 1964), it is even more likely that this proximity is more than mere coincidence. It is possible that the areas of large curvature are specifically used to optimize the

transduction of orientation and movement, especially since the direction of largest curvature and the direction of hair cell polarization coincide there.

4.1.2 High-frequency responses of the otolith structure. Our results indicate that the properties of the interotoconial matrix might allow resonances. We propose such a process since it was found that intense impulsive noise and vibration of the inner ear lead to long-term impairment and damage of the otoliths (Perez et al. 2002; Otsuka et al. 2003). As noted above, the model of the otoconial layer used in this investigation includes substantial simplifications, especially with respect to the distribution of the otoconia. The mechanical properties of the material filling the interotoconial space are further unknown. It is thus important to emphasize the model character of this investigation. Nevertheless, we have included it here since it demonstrates how the otoconial layer may be affected by vibrational stimuli and predicts that there is a most effective frequency range, and gives an estimate of where this range might be found. There probably also exist other mechanisms that could account for the damage to this layer, like vibration of the otoconia with respect to each other. We chose this approach since shear displacements of the otoconial layer may represent the natural response of the structure to movements of the head. Ultimately, experiments that monitor vibrational frequencies are needed to understand which processes damage the otoliths.

Crucial to the resonance frequency is the elasticity of the interotoconial matrix, E_{int} (assuming linear material properties). Since no experimental data are available about the possibly nonlinear stress-displacement relationship, our estimate relies on the observation that the rigidity of this matrix is much smaller than that of the mesh layer. The resonance frequency for lightly damped materials is related to the parameter by a square law

$$f_{\text{Res}} \propto \sqrt{E_{\text{int}}} \ . \tag{6}$$

This ensures that, even if the elasticity is wrong by a factor of 10, the resonance frequency will only shift by a factor of 3. Assuming that the elasticity of the gel layer is typical for a ''weak'' inner-ear material and the error associated with the elasticity of the material is of this order, we estimate that the resonance frequency falls into a range of between 100 Hz and 2 kHz. Even if the elasticity is similar in all parts of the otoconial layer, it is well known that otoconia have considerably different masses: otoconia from the extrastriola region are larger than those from the striola. For this reason, no single resonance frequency can be expected. Instead, it is more likely that a whole band of resonance frequencies exists for the different parts of the otolith membrane.

While the mass of the otoconia and the elasticity of the interotoconial matrix determine the resonance frequency, the damping provided by the fluid-filled interotoconial matrix specifies how pronounced the resonance is. If the damping were stronger than assumed in our simulations, the amplitude of the resonance would decrease. For an overdamped system, the resonance would vanish completely. If, on the other hand, the fluid-filled interotoconial matrix were not strong enough to provide such a large magnitude of damping, oscillating acceleration in this frequency range could lead to harmful results. Due to their different masses, different parts of the otoconial layer oscillate with different phase relations. This would result in large stresses within the interotoconial matrix and could ultimately lead to a damage of the structure. Such a process might induce benign paroxysmal positional vertigo. Resonances of the otoconia may also be linked to reports about disorientation and stranding of whales and dolphins in areas where low frequency active sonar has been used. The frequencies employed in this kind of sonar (about 100–500 Hz) fall into the frequency range where otoconial resonances may be expected. While it is accepted that the high levels of sound used in these surveillance systems significantly impair the hearing of crustaceans, our simulations suggest an additional mechanism for these observations, provided that the mechanical properties of the otolith structure in dolphins and whales is similar to that of other mammals.

4.2 Hair cell responses

Many units in the extrastriola region exhibit tonic responses (Goldberg et al. 1990a). The response patterns elicited by time-dependent, linear accelerations in these units are therefore similar to the ones elicited by corresponding, static linear accelerations. In contrast, the tonic-phasic units in the striola provide additional dynamic information. The narrow shape of the striola allowed us to characterize these units by their location along the striola. The right column in Fig. 5 shows the time course of responses over the striola for different directions of head tilts. Since responses to sensory inputs are most likely optimized for everyday movements, we used natural, small head tilts of 10°. The response patterns arising from tilts in different directions can vary substantially (Figs. 5d and f).

Although both response patterns in Figs. 5d and f are due to 10° tilts, left ear down tilts seem to be more effective since the amplitudes are larger. The dynamic responses are a mixture of tonic and phasic components. During movements these components lead to a maximum response that decays to the tonic state corresponding to the new head position. In our model, peak responses occur simultaneously on different locations of the striola. This indicates that the mechanical properties of the otolith structure induce no time delays in the displacement between different parts of the striola, and no information on tilt direction is coded in the temporal shape of the response. Also, the temporal decay of the patterns yields no information on the tilt direction. As Fig. 5b shows, the time course of the decay from the maximum to the tonic state is similar throughout the striola. Both observations support the assumption that tilt directions might be coded as spatially distributed response patterns. This is shown in Figs. 6a and b,

where maximum responses were calculated for different tilt directions of the head. For both utricle and saccule, different tilt directions lead to distinctly different response patterns. Thus the direction of head tilt uniquely determines the response pattern.

At this point we can only speculate as to how the information about orientation and movement is coded in these patterns. For example, simply integrating the overall response along the striola may provide information about the direction of head tilts (Figs. 6c and d). These results also indicate that the saccule can contribute significantly to the detection of head movements about the upright orientation. Though the maximum responses are generally smaller for the saccule, they are still a large fraction of the corresponding value for the utricle. Interestingly, summed maximum responses of the left and right saccule are in the 45°/225° and 135°/315° direction, respectively (Fig. 6d). These summed responses are thus in similar planes as the superior and posterior lateral semicircular canals, suggesting a simple mechanism for interactions between cumulative saccular responses and afferent signals from the angular velocity sensors.

Acknowledgements. This study was supported by DLR 50WB9940 and by the Betty and David Koetser Foundation for Brain Research. We also want to thank A. Kondrachuk and C. Bockisch for their thorough and helpful comments on the manuscript.

References

Benser ME, Issa NP, Hudspeth AJ (1993) Hair-bundle stiffness dominates the elastic reactance to otolithic-membrane shear. Hear Res 68: 243–252

Blanks RH, Curthoys IS, Markham CH (1975) Planar relationships of the semicircular canals in man. Acta Otolaryngol 80 (3–4): 185–196

Carlström D, Engström H, Hjorth S (1953) Electron microscope and x-ray diffraction studies of otoconia. Laryngoscope 63: 1052–1057

Curthoys IS, Betts GA, Burgess AM, MacDougall HG, Cartwright AD, Halmagyi GM (1999) The planes of the utricular and saccular maculae of the guinea pig. Ann NY Acad Sci 871: 27–34

Damiano ER, Rabbitt RD (1996) A singular perturbation model of fluid dynamics in the vestibular semicircular canal and ampulla. J Fluid Mech 307: 333–372

Fernandez C, Goldberg JM (1976) Physiology of peripheral neurons innervating otolith organs of the squirrel monkey: II. Directional selectivity and force-response relations. J Neurophysiol 39: 985–995

Fernandez C, Goldberg JM, Abend WK (1972) Response to static tilts of peripheral neurons innervating otolith organs of the squirrel monkey. J Neurophysiol 35: 978–997

Flock A (1964) Structure of the macula utriculi with special reference to directional interplay of sensory responses as revealed by morphological polarization. J Cell Biol 22: 413–431

Goldberg JM, Desmadryl G, Baird RA, Fernandez C (1990a) The vestibular nerve of the chinchilla: IV. Discharge properties of utricular afferents. J Neurophysiol 63: 781–790

Goldberg JM, Desmadryl G, Baird RA, Fernandez C (1990b) The vestibular nerve of the chinchilla: V. Relation between afferent discharge properties and peripheral innervation patterns in the utricular macula. J Neurophysiol 63: 791–804

Grant JW, Best WA (1987) Otolith-organ mechanics: lumped parameter model and dynamic response. Aviat Space Environ Med 58: 970–976

Grant JW, Cotton JR (1990) A model for otolith dynamic response with a viscoelastic gel layer. J Vestib Res 1: 139–151

Grant JW, Huang CC, Cotton JR (1994) Theoretical mechanical frequency response of the otolithic organs. J Vestib Res 4: 137–151

Hackney CM, Furness DN (1995) Mechanotransduction in vertebrate hair cells: structure and function of the stereociliary bundle. Am J Physiol Cell Physiol 37: C1–C13

Hess BJM (1992) Three-dimensional head angular velocity detection from otolith afferent signals. Biol Cybern 67: 323–333

Howard J, Hudspeth AJ (1987) Mechanical relaxation of the hair bundle mediates adaptation in mechanoelectrical transduction by the bullfrog's saccular hair cell. Proc Natl Acad Sci USA 84: 3064–3068

Jaeger R, Takagi A, Haslwanter T (2002) Modeling the relation between head orientations and otolith responses in humans. Hear Res 173: 29–42

Kachar B, Parakkal M, Fex J (1990) Structural basis for mechanical transduction in the frog vestibular sensory apparatus: I. The otolithic membrane. Hear Res 45: 179–190

Kondrachuk AV (2000) Computer simulation of the mechanical stimulation of the saccular membrane of bullfrog. Hear Res 143: 130–138

Kondrachuk AV (2001a) Finite element modeling of the 3D otolith structure. J Vestib Res 11: 13–32

Kondrachuk AV (2001b) Models of the dynamics of otolithic membrane and hair cell bundle mechanics. J Vestib Res 11: 33–42

Lindeman HH (1969) Studies on the morphology of the sensory regions of the vestibular apparatus. Ergeb Anat Entwicklungsgesch 42: 1–113

Lins U, Farina M, Kurc M, Riordan G, Thalmann R, Thalmann I, Kachar B (2000) The otoconia of the guinea pig utricle: internal structure, surface exposure, and interactions with the filament matrix. J Struct Biol 131: 67–78

Money KE, Bonen L, Beatty JD, Kuehn LA, Sokoloff M, Weaver RS (1971) Physical properties of fluids and structures of vestibular apparatus of the pigeon. Am J Physiol 220: 140–147

Otsuka K, Mamoru S, Masayoshi F (2003) Model experiment of benign paroxysmal positional vertigo mechanism using the whole membranous labyrinth. Acta Otolaryngol 123: 515–518

Perez R, Freeman S, Cohen D, Sohmer H (2002) Functional impairment of the vestibular end organ resulting from impulse noise exposure. Laryngoscope 112: 1110–1114

Rao SS (1982) The finite element method in engineering. Pergamon, Oxford

Ross MD, Komorowski TE, Donovan KM, Pote KG (1987) The suprastructure of the saccular macula. Acta Otolaryngol 103: 56–63

Sato H, Sando I, Takahashi H (1992) Computer-aided three-dimensional measurement of the human vestibular apparatus. Otolaryngol Head Neck Surg 107: 405–409

Shotwell SL, Jacobs R, Hudspeth AJ (1981) Directional sensitivity of individual vertebrate hair cells to controlled deflection of their hair bundles. Ann NY Acad Sci 374: 1–10

Takagi A, Sando I (1988) Computer-aided three-dimensional reconstruction and measurement of the vestibular end-organs. Otolaryngol Head Neck Surg 98: 195–202

Trincker D (1962) Transformation of mechanical stimulus into nervous excitation. Soc Exp Biol Symp 16: 131–141

Viirre E, Demer JL (1997) Head and eye in three dimensions during standing, walking and running. In: Fetter M, Haslwanter T, Misslisch H, Tweed D (eds) Three-dimensional kinematics of eye, head and limb movements. Harwood, Amsterdam, pp 217–223